Alkali Activation of Ladle Slag from Steel-Making Process

Elijah Adesanya[1], Katja Ohenoja[1], Paivo Kinnunen[1], and Mirja Illikainen[1]

[1]*Fibre and Particle Engineering Unit, PO Box 4300, University of Oulu, 90014, Finland*

Corresponding Author: Mirja Illikainen *Mirja.illikainen@oulu.fi +358405885904*

Abstract. Ladle slag, a currently under-utilized crystalline metallurgical residue was studied for use as a precursor for alkali activation. An activating solution containing sodium silicate and potassium hydroxide was used in activating the slag with varying compositional ratios in order to optimize the compressive strength. Ladle slag is commonly regarded as having limited reaction with alkalis, and in previous studies it has been therefore mixed with reactive precursors, such as metakaolin. However based on our results ladle slag shows potential as a sole precursor for alkali activated binders. X-ray diffractometry reveals that the major minerals in the ladle slag were identified to be γ-dicalcium silicate and mayenite. After alkali activation, the major reaction product was a silicate hydrate according to DRIFT analysis, sodium substituted calcium aluminosilicate hydrate gel, C-(N)-A-S-H. XRD analysis support the hypothesis by revealing an amorphous "halo" in the alkali activated slag. The unconfined compressive strength of the optimized alkali-activated ladle slag paste specimen was 65 MPa after 28 days.

Keywords: Reuse, crystalline slag, ladle slag, Alkali activation mayenite, strength

Introduction

Increased generation of industrial residues from iron and steel making has prompted the industrial sector and the research community to search for new ways to utilize these by-products in order to reduce the amount of landfilled residues. These residues and by-products include ground granulated blast furnace slag (GGBFS), desulphurization slag (De-S), converter slag and ladle slag (LS), also known as falling slag.

In 2012, approximately 21 million tons of slag was generated in Europe from steel-making processes. About 65% of this amount is utilized in different fields (i.e. cement production, road construction, etc.) [1]. Exact numbers on ladle slag production are scarce, however by assuming that 12-15 kg of unrecyclable ladle slag is produced for every 1000 kg of crude steel, and 160 Mt of annual crude steel production, we arrive at an estimated 1.9-2.4 Mt of yearly ladle slag production in Europe. Serjun *et al*. [2], reported that about 80% of LS generated in the Europe is either landfilled or stored. Various researchers have proposed an alternative use of LS as fillers in self-compacting concrete and in masonry mortars [3–5], and also in landfill covering as filtering beds and in stabilizing soft clayey soils [2, 6]. The chemical composition of LS varies according to the steel-making factories' processes, conditions and additives; however, the composition includes CaO, SiO_2, Al_2O_3 and MgO, which makes this slag a potential binder in alkali activation [7].

Alkali-activated slag (AAS), generally made of GGBFS, is a promising construction material with similar or better properties than ordinary Portland cement (OPC) in terms of its high strength, durability and CO_2 footprint [8–11]. Different researchers [11–13] have reached the consensus that when activated with alkaline solution, the main reaction product in a calcium-rich slag is a poorly crystalline calcium silicate hydrate with aluminum (C-A-S-H gel) in its composition, which is responsible for the strength development. The gel also includes a significant amount of Na in specific charge-balancing sites, and therefore, the gel structure can also be written as C-(N)-A-S-H [14, 15]. The gel in AAS differs from OPC-hydrated gel, as it has a low Ca/Si ratio, showing a dissimilar structure [16].

LS, unlike other widely studied raw materials for alkali activation, is predominantly crystalline in nature due to the high basicity and slow cooling procedures from the furnaces; the crystalline phases commonly observed are dicalcium silicate (γ-C_2S), mayenite ($Ca_{12}Al_{14}O_{33}$), gehlenite $Ca_2(Al(AlSi)O_7)$ and traces of periclase (MgO) [22]. Despite the high degree of crystallinity of LS, a number of publications have been reported on the alkaline activation of similar crystalline slags [19–23]. Kriskova *et al.* [21, 22] showed that the hydraulic potential of a crystalline slag could be improved through mechanical and chemical activation. Salman *et al.* [23], studied the hydraulic potential of argon oxygen decarburization (AOD) slag in alkali solutions. The authors observed, using XRD, a considerable reduction in the crystalline peaks and an increment in the amorphous content of the activated

slag at 90 days. Also, they achieved a 90-day unconfined compressive strength (UCS) of 31 MPa. In other studies on crystalline slags, Salman *et al.* [19] derived considerable compressive strength of around 40 MPa after 90 days of curing for alkali activated stainless steel refining (SSR) slag.

However, to the best of our knowledge, no reports exist regarding alkali activation of LS as a sole binder source. In related studies, researchers used LS as a co-binder with other aluminosilicate materials in alkali activation, and they found that it reacted and participated in the gel formation [24–27]. This present study aims to investigate the possibility of activating LS as the sole precursor in alkali-activated cementitious material as a method of utilizing it. The synthesis of alkali activated LS by changing the chemical composition of the binder and the alkali solutions was done in order to achieve high compressive strength. The mechanical strength, porosity and water absorption of the samples were measured. The activated materials were further characterized by using microstructural and mineralogical analyses.

Materials and Experimental Methods

Materials

The LS was supplied by SSAB, Finland. The as-received slag was collected prior to being exposed to air humidity or rainy weather. The fraction used in this study was an un-milled fine fraction below 8 mm and had a d_{50} value of approximately 57 µm. The alkaline activating solution was composed of chemical grade sodium silicate (Na_2SiO_3) with a modulus M_s (SiO_2/Na_2O) = 3.5 containing 66.5% of water. Potassium hydroxide (KOH) pellets supplied by Merck KGaA chemicals. Potassium hydroxide was used to supplement Na in order to lower the viscosity of the activating solution. In addition, diatomaceous earth (DE), with a median particle size of 18.16 µm, was used as a silica source, and distilled water were added to obtain a specific mix design. In the activating solution with DE, it was observed that it was not completely soluble, this was visually evident with the sedimentation of some DE particles in the solution. The activating solutions were prepared a day prior to activating the LS so as to ensure solution equilibration.

The chemical composition of the LS in Table 1 was determined with 4KV XRF (PANalytical Omnian Axiosmax). The free CaO was 0.0, measured using the method described in the standard EN 450-1.

Table 1. Chemical composition (wt.%) of LS used measured with XRF and given as oxides.

Oxides	CaO	SiO_2	Al_2O_3	Fe_2O_3	MgO	SO_3	Others
LS	49.8	10.1	27.1	1.1	6.4	1.1	4.4

Slag fineness plays a key role in the dissolution of chemical components of slag [28, 29], and the alkali activation of LS could be enhanced by reducing the particle size. Therefore, the received LS was milled to achieve a d_{50} value of less than 10 µm in dry mode using a 10 L roller ball mill chamber (Germatec, Germany) and with a grinding media filling ratio of 60%. Then, 2 kg of the slag was milled for 2 hours after which the milled LS particles above 90 µm were sieved out using a vibrating sieve shaker, the Analysette 3 (Fritsch, Germany), at an amplitude of 0.5 mm for 5 minutes. The particle size distribution of the milled LS was analyzed using a laser diffraction technique (Beckman Coulter 13320) with the Fraunhofer model. Isopropanol was used in the technique rather than water to avoid reaction of the slag sample during analysis. The specific surface area of the milled LS was determined by physical adsorption of gas molecules to a solid surface measured using a Micromeritics ASAP 2020 instrument and the results were reported as the Brunauer–Emmett–Teller (BET) isotherms.

Experimental Methods

The optimum alkaline content ($Na_2O_{equivalent}$) required to achieve good strength was first determined. In this experiment, the CaO/SiO_2, SiO_2/Al_2O_3 molar ratios and water-to-solid (w/s) mass ratios were kept constant. The w/s was taken as the ratio of the total water content to the solid content (g/g). The Na_2O_{eq} was calculated as the combination of the alkali content of (Na_2O+K_2O) using the following equation:

$$Na_2O_{eq}\ (\%) = Na_2O\ (\%) + (62.0/94.2) \times K_2O\ (\%) \quad (1)$$

In the second set of experiments, the silica concentration was varied while keeping w/s, CaO/Na_2O_{eq} and Al_2O_3/Na_2O_{eq} constant. The formulation was done by choosing the mix design from the first phase with the highest compressive strength (Na4.3 in Table 2 & 3) and adjusting the silica content from 15 % to 22 % (Table 4 & 5).

The silica content was increased by initially increasing the sodium silicate and then by adding DE to achieve similar ratio parameters while also keeping the w/s constant. The water-to-solid (w/s) ratio of 0.40 in all mixes was kept constant.

Table 2. Mix design of AALS samples in wt% for varying alkali concentrations.

	Na-Silicate (dry matter)	KOH (dry matter)	H_2O (total)	LS
Na4	15.0	0.0	28	56.5
Na4.3	14.6	1.8	28	55.1
Na5.6	14.3	3.6	28	53.8
Na6.3	13.9	5.2	28	52.4
Na7.6	13.6	6.8	28	51.2

Table 3. Resulting composition of the alkali metal variations in molar ratios.

Molar ratios	Na4	Na4.3	Na5.6	Na6.3	Na7.6
$(Na_2O + K_2O)/SiO_2$	0.19	0.26	0.33	0.39	0.46
SiO_2/Al_2O_3	1.88	1.88	1.88	1.88	1.88
$H_2O/(Na_2O + K_2O)$	27.6	20.8	17.0	14.4	12.6
CaO/SiO_2	1.64	1.64	1.64	1.64	1.64

Table 4. Mix design of AALS samples in wt% for varying silica concentrations.

	Na-Silicate (dry matter)	KOH (dry matter)	H_2O (total)	LS	DE
Na4.3Si15	10.7	3.6	28	57.4	0.0
Na4.3Si16	12.5	2.8	28	56.7	0.0
Na4.3Si17	13.5	2.4	28	56.1	0.0
Na4.3Si20	14.8	1.6	28	52.8	2.4
Na4.3Si22	14.9	1.4	28	50.8	4.5

Table 5. Resulting composition of the silica content variations in molar ratios.

Molar ratios	Na4.3Si15	Na4.3Si16	Na4.3Si17	Na4.3Si20	Na4.3Si22
$(Na_2O + K_2O)/SiO_2$	0.33	0.29	0.28	0.22	0.20
SiO_2/Al_2O_3	1.52	1.67	1.77	2.23	2.54
$H_2O/(Na_2O + K_2O)$	19.5	19.9	19.9	21.3	22.1
CaO/SiO_2	2.02	1.84	1.74	1.38	1.21

All alkali-activated ladle slag (AALS) specimens were prepared by mixing the LS and the alkaline activator in a planetary mixer (THINKY Corporation ARE-250, England) for 1 minute at 2000 rpm to achieve a homogenous paste. The resulting pastes were casted in polypropylene cylindrical molds (25 mm in diameter and 20 mm in height) and were vibrated on a vibrating machine (Vortex-Genie 2, Prolab Oy) to remove entrained air. Samples were then placed in a tightly sealed plastic bag and cured for 24 hours at 60° C. Then, samples were demolded and cured in a sealed bag at room temperature prior to testing.

Characterization Methods

Configured with Cu-Kα radiation (40 mA and 40kV), x-ray powder diffraction (XRD) (Siemens D500 AG, Germany) was used to collect the diffraction patterns of the unreacted LS and the activated samples, which were then compared with matching diffraction patterns from the ICDD database (The International Centre for Diffraction Data 2006). The diffraction pattern of each sample was derived with a step interval of 0.04°/step, a count step of 2.5 s/step and an angle interval range of 10–60°. Diffuse reflectance infrared Fourier transform (DRIFT) was used to characterize the raw LS and some selected AALS. The spectra were collected with a Bruker Vertex 80v spectrometer (USA) for the samples. Spectra were obtained in the 400–4000 cm−1 range, and 40 scans were taken at a resolution of 1 cm^{-1} for each sample. The DRIFT was done on 273 days old samples.

FESEM analysis were undertaken with a Zeiss Ultra Plus instrument (USA). For the activated samples, polished SEM samples were prepared by impregnating the dried crushed samples (273 days old) in epoxy and then polished to a very smooth surface. All the samples were sputter coated with carbon to create a conductive layer over the

surface. These microstructure analyses were conducted in order to analyze the morphology of the LS and activated samples.

Compressive strength was determined after 28 days using an Instron 8500 compression-testing machine (firmware v35.0 with a maximum load of 200 kN) with a loading force of 2.4 kN/s. Four to five samples of each mix design were tested, reporting their average value as the compressive strength. The water absorption test was conducted according to SFS 5513 [30]: the samples were dried in the oven at 105 °C for 48 hrs and then weighed (M_d) after. Samples were then immersed in water for 72 hrs, removed from the water and dried with a damp cloth before being weighed (M_w) separately. Water absorption was reported as the percentage increase in weight.

Porosity (P) was estimated with envelope (ρ_E) and skeletal densities (ρ_S) using using Eq. 2. Envelope density was measured by the mass of each cylindrical bulk sample over its geometric volume; the skeletal density was determined by analyzing ground AALS samples using helium gas pycnometer (Micromeritics, USA).

$$P = (1 - {}^{\rho_E}/_{\rho_S}) \text{ x } 100 \quad (2)$$

Results and Discussion

Ladle Slag

The median particle size d_{50} was 9.13 µm, as determined with the laser diffraction particle size analyzer for milled LS. The BET surface area was 674.1 m^2/kg. Major components presented in Table 1 include CaO, Al_2O_3 and SiO_2. From these values, it is possible to calculate the Al_2O_3/SiO_2 ratio of 2.70, the CaO/SiO_2 ratio of 4.90 and a basicity coefficient [Kb = (CaO + MgO)/(SiO_2 + Al_2O_3)] of 1.4. Typically, slags are classified into three groups based on this coefficient as follows: acid (Kb < 1), neutral (Kb = 1) and basic (Kb > 1). LS used in this study is therefore basic, which is preferable in alkaline activation [31, 32]. Fig. 1 presents an FESEM image of LS milled for 2 hours with a ball mill. The slag particles seem to be partially agglomerated, showing a wide particle size distribution with irregular and sharp-shaped particles. The particle size ranges from around 2 µm to 25 µm. Fig. 2 illustrates the particle size distribution, showing the distribution of the milled LS used in the experiment. In Fig.3, the mineralogical properties of the raw milled LS is presented. The diffractogram shows a highly crystalline material with major phases detected including mayenite ($Ca_{12}Al_{14}O_{33}$) and gamma dicalcium silicate (γ-C_2S, $Ca_2(SiO_4)$) and traces of periclase (MgO).

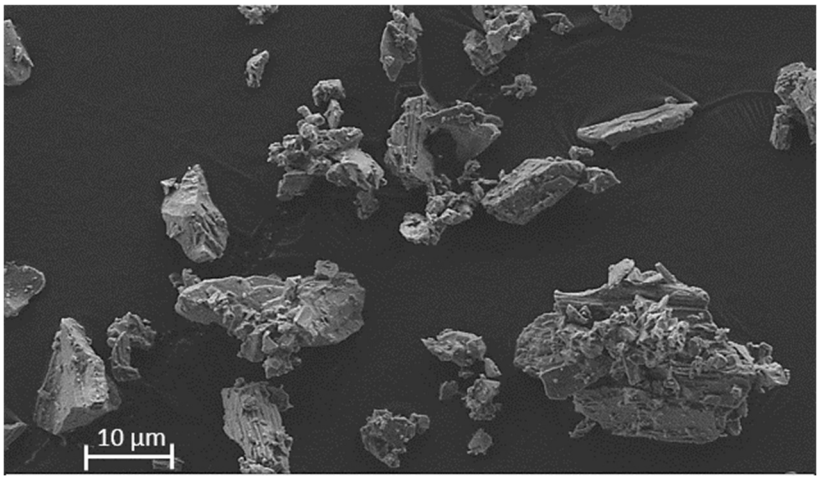

Fig. 1. FESEM image of original LS after 2 hours of grinding.

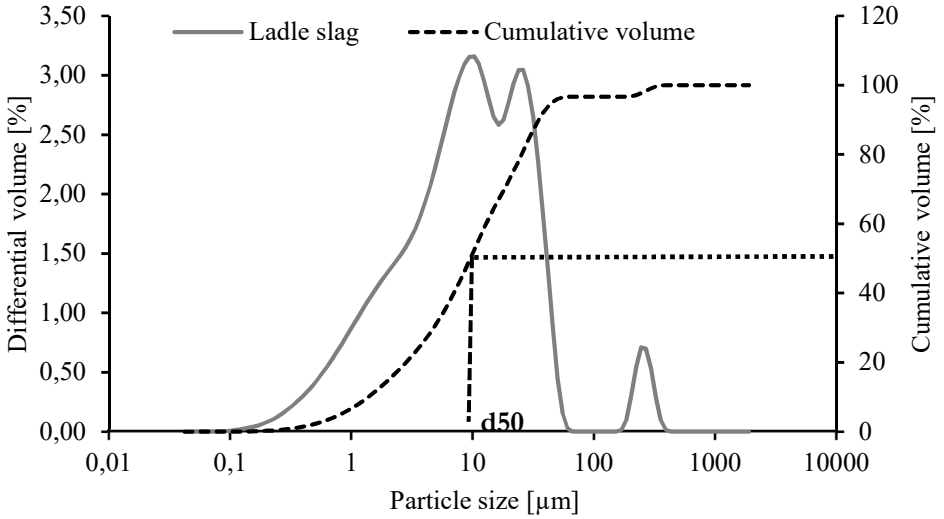

Fig. 2. Particle size distribution of the milled LS.

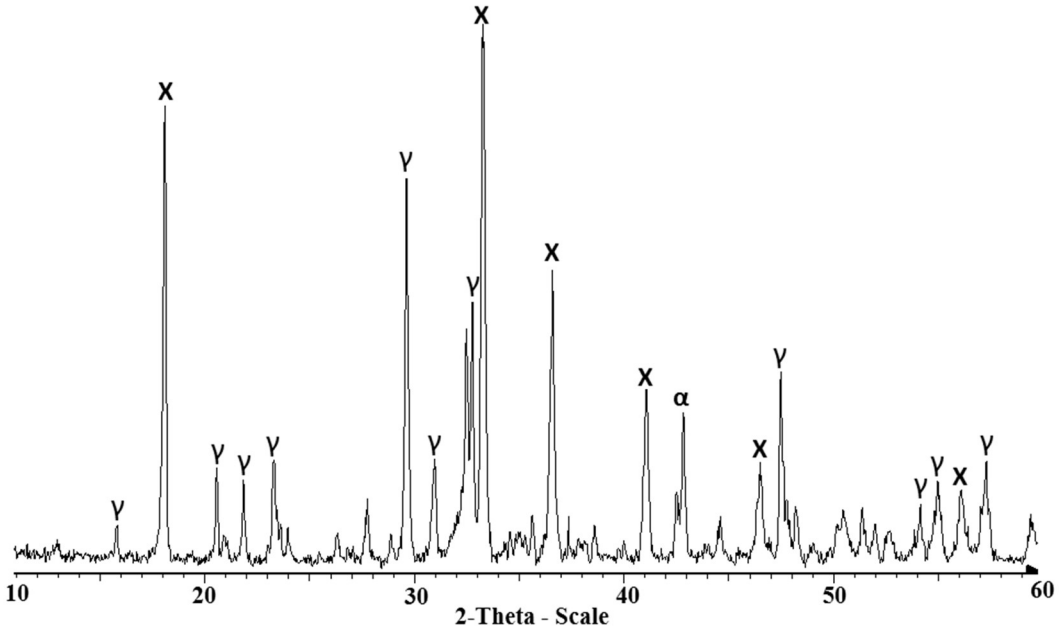

Fig. 3. X-ray graph of the milled LS. Peaks marked are gamma dicalcium silicate (γ), mayenite (x) and periclase (α).

Properties of the Fresh and Hardened Alkali-Activated Materials

Tables 2 and 4 report the mix design for each LS sample. AAS materials are prone to quick setting during mixing, which was also the case for LS studied in this research; Na4.3 and Na7.6 sets rapidly. This phenomenon is attributed to one of the primary crystalline phase of the LS identified as Dodecacalcium hepta-aluminate ($C_{12}A_7$) or mayenite. It is a reactive starting phase in high-aluminum cements that reacts rapidly in a few minutes in contrast to other calcium aluminate phases, such as calcium monoaluminate and calcium dialuminate [34, 35]. The setting time was analyzed visually, and it was observed that it increased with increasing KOH content (from Na4.3 to Na6.3). It should be noted that during testing and analysis, cracking defects were not visibly apparent on tested specimen; however, the occurrence of microcracks cannot be disregarded and might have influenced the results.
AASs are known to have higher drying shrinkage compared with OPC [36, 37]. In a previous study on alkali activation of AOD stainless steel slag, the authors observed microcracks during the microstructural analysis of the activated stainless steel slag [23].

XRD Analysis

In Fig.4, the XRD patterns were analyzed for some selected AALS samples (Na4.3 and Na4.3Si20) and compared with the starting milled LS pattern. The AALS samples were chosen based on their strength gain.
It is revealed from the diffraction pattern of both AALS samples, that there is an increase in the amorphous phase with a weak amorphous "halo" from 23 to 38° 2θ when compared with the raw slag. This increased amorphous phase implies that some constituents of the LS have dissolved in the alkaline solution, leading to the formation of an amorphous hydration product likely C-(N)-A-S-H gel. The C-(N)-A-S-H gel is a likely reaction product even though the amorphous halo is overlapped by the peaks of dicalcium silicate and mayenite hydrate and is supported by the DRIFT analysis in the following section. Similar observations have been reported for EAF slag and LS in alkaline solution [17, 38].
Furthermore, this development in the phase evolution of the samples shows the potential of crystalline slag reactivity in alkaline solution. The considerable factor is the existent of mayenite as one of the main minerals; this calcium aluminate mineral is known to react rapidly [35]. Also, it should be noted that some peaks in the patterns were not identifiable, notably at 48.5 and 60 2θ.

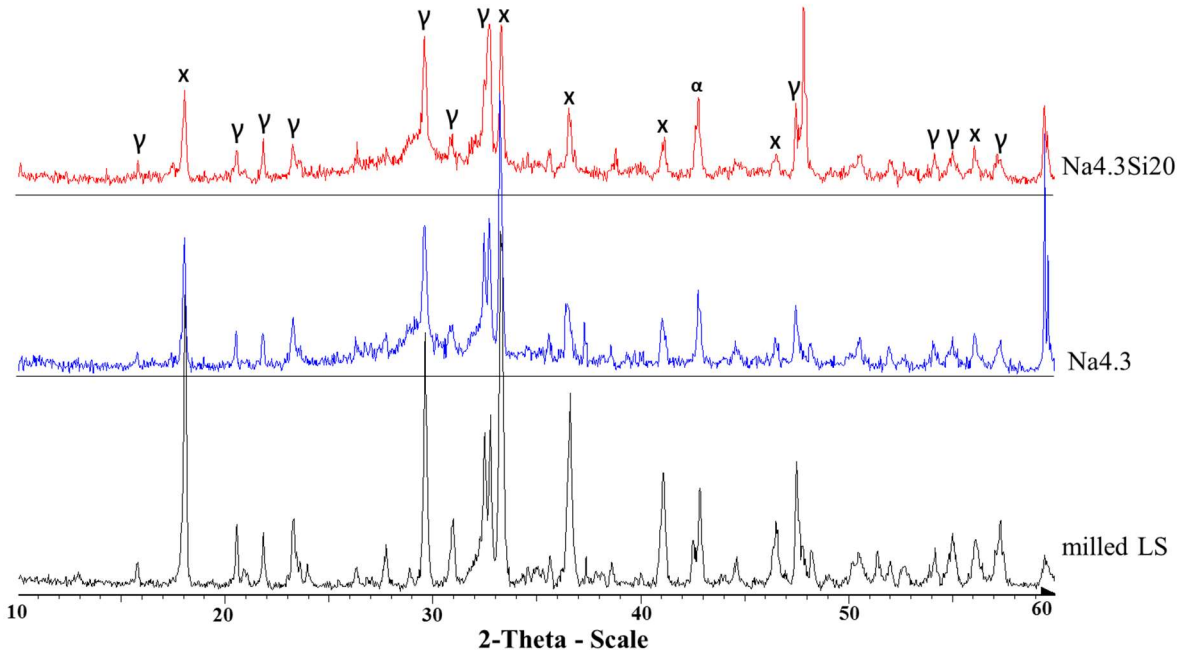

Fig. 4. XRD graphs of milled LS and AALS after 28 days: Na4.3 and Na4.3Si20 (γ: γ-C_2S, x: Mayenite and α: Periclase).

DRIFT Spectral Analysis

Fig. 5 shows the infrared spectra of raw slag (non-hydrated LS), DE and selected activated samples. All activated samples' infrared spectra are similar with no major differences. The vibration bands at 1648 cm^{-1} in activated samples is due to H-O-H bending vibrations, and indicates the presence of water in the hydration product, while not present in the starting material [39]. The peaks around 1030 – 1101 cm^{-1} correspond to the asymmetric stretching vibration of the Si-O bonds [40]. The spectra shows the shift in position of the stretched vibration bands of the Si-O bonds from 1030 cm^{-1} in the unhydrated slag to 1101 cm^{-1} in the activated slag; the increase in wavenumber and the broadness of the bands with the increase in the silica content in the activated slag is linked to the formation of a polymerized Si-O network, [40, 41] with amorphous structure.
Also, the spectra show a low intensity absorption band at around 600 cm^{-1} which has been associated with the vibration of T-O_4 groups (T represents tetrahedral Si or Al) [41, 42].
The absorbance peaks at 1648 cm^{-1} and a broad peak around 1071 cm^{-1} share great resemblance with a mixture of C-S-H and N-A-S-H gels studied by Garcia-Lodeiro *et al.* [43]. The remaining wide absorption bands at 1406-1482 cm^{-1} correspond to asymmetric stretching vibrations of O-C-O bonds of carbonates group [23, 44], which suggests that carbonation of the sample had occurred during the long curing period, since carbonate phases were not observed after 28 days of curing (using XRD).

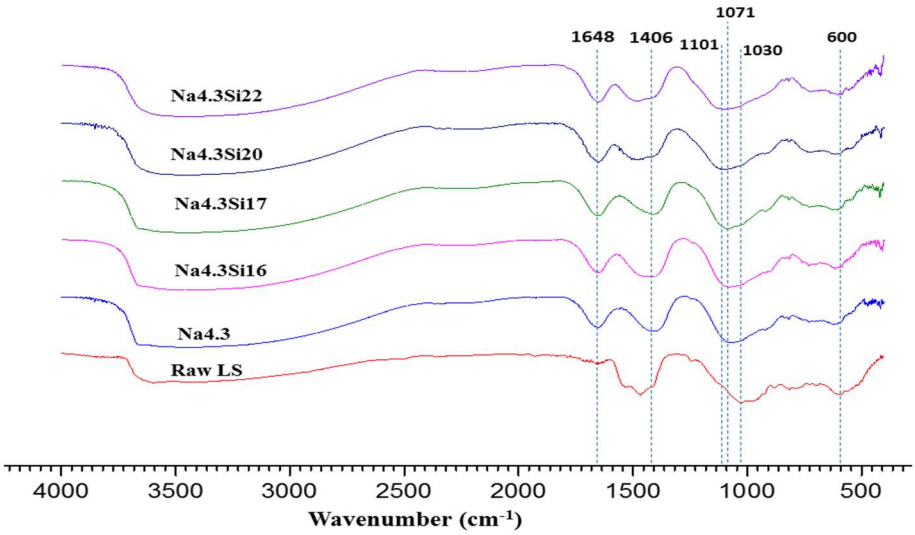

Fig. 5. FTIR spectra of unhydrated LS and selected activated samples at 273 days.

FESEM analysis

SEM analysis undertaken on the polished surfaces of the selected AALS paste samples are presented in Figs. 6(a) and 7(a), revealing unreacted slag grains imbedded in matrix. Both samples show microcracks. Narrow reaction ring can be observed at the interface between the unreacted grains and the alkali activated paste. At higher magnification, the microstructure of the AALS pastes can be seen in Figs. 6(b) and 7(b).

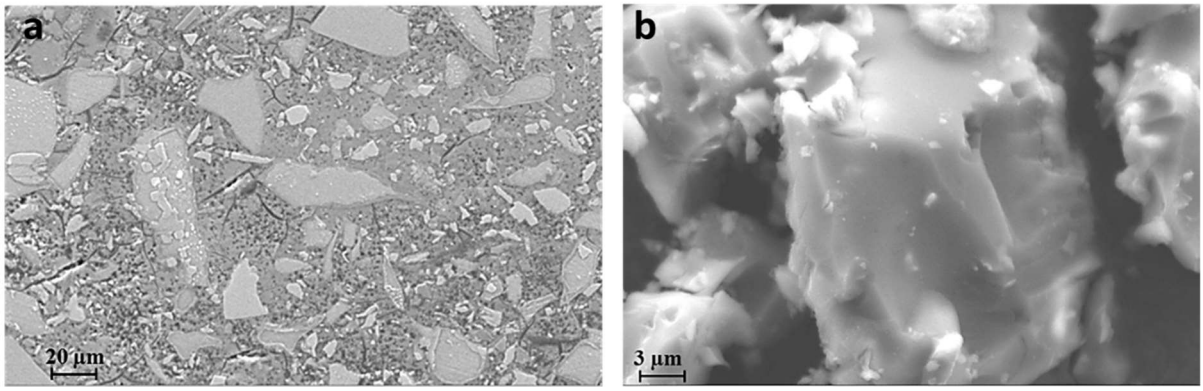

Fig. 6. SEM image of Na4.3 paste of (a) polished and (b) ground AALS sample.

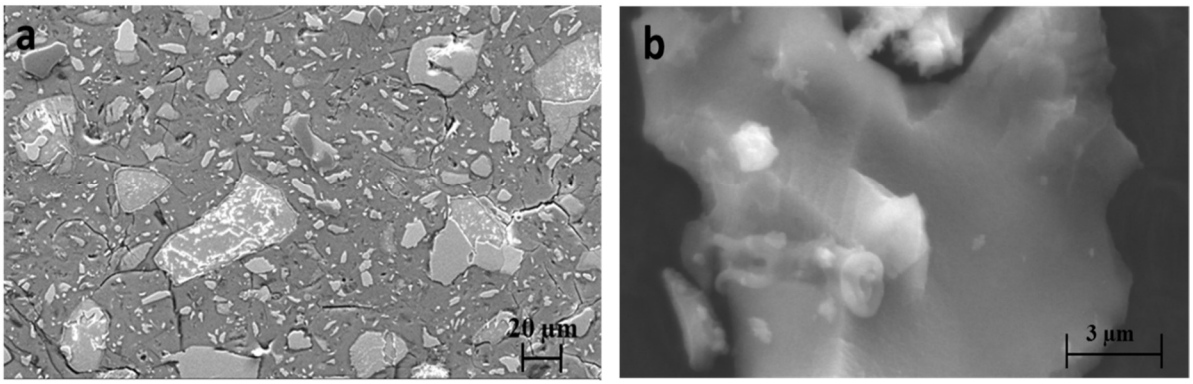

Fig. 7. SEM image of Na4.3Si20 paste of (a) polished and (b) ground AALS sample.

Mechanical Properties of AALS samples

The Effect of Na_2Oe_q Concentrations on the Compressive Strength

During alkali activation, alkali hydroxides promotes dissolution of the chemical components in the slag particles, thereby increasing the formation of hydration products. The effect of increasing Na_2Oe_q concentration in the paste mix was investigated in relation to strength development. Fig. 8 presents the average UCS as a function of Na_2O_{eq} concentration. In this study, the increased alkali hydroxides concentration seemed to slightly decrease the strength or maintain it within the same value, although with low confidence due to error sources (i.e. size of the specimens, the presence of microcracks). Na4.3 achieved the highest compressive strength of 47 MPa after 28 days. The lowest compressive strength of 38 MPa after 28 days occurred in Na6.3.

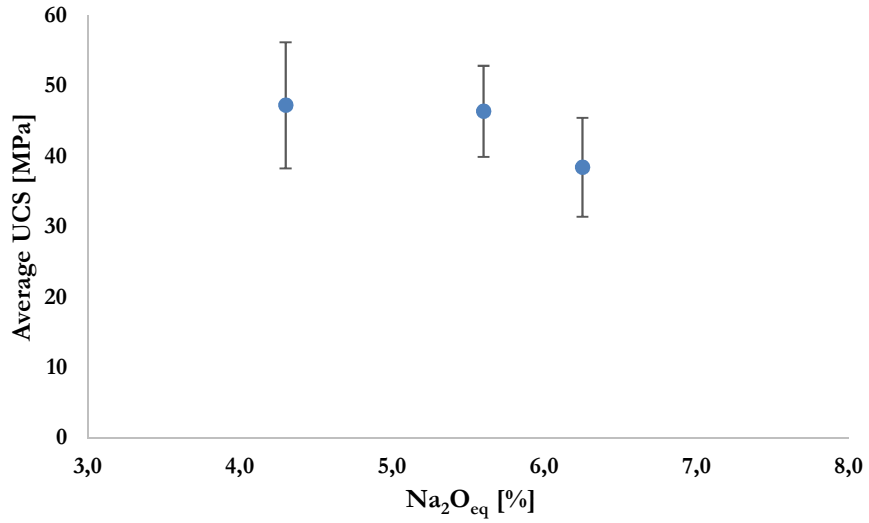

Fig. 8. Effect of Na_2Oe_q concentrations on compressive strength of AALS.

This slight decrease in compressive strength with increasing alkali content may be due to excess alkaline metals (K^+ and Na^+) in the AALS paste. Excess alkaline metals in alkali activated materials have been reported to precipitate in the binder gel (C-A-S-H) in the early stage of hydration, deterring further formation of binder phases and thereby decreasing strength [45, 46]. During the curing period of the AALS samples, the present study also observed that high-alkaline specimens (Na5.6 and Na6.3) exhibited crystalline deposits on their surface, potentially efflorescence resulting from excess alkaline contents in the mix. No precipitates were observed on the Na4.3 samples. Some studies have reported on the negative effects of efflorescence on the compressive strength of geopolymers [47], however this can hardly play a major role due to relatively low Na/Al -ratios in our samples (0.49). More likely, microcracks seen from the SEM pictures in Fig. 6 and 7, could be a major factor in the reduced strength of higher alkali samples.

The Effect of Silicate Content on Compressive Strength

Fig. 9 presents the average UCS as a function of silicate modulus. For this aspect, the silica content was varied and each mix was designed according to the molar composition of Na4.3 presented in Table 3. In two of the samples (Na4.3Si20 and Na4.3Si22), the silica content was increased by adding DE at 5 and 8 wt.% of the slag, respectively. As illustrated in Fig. 9, the compressive strength increased with increasing silica content until it reached a SiO_2 content of 20% after which it plateaued. Optimal silica concentration seems to be then 20%. Another factor may be the pozzolanicity of DE, which has been shown in cementitious systems [48, 49].

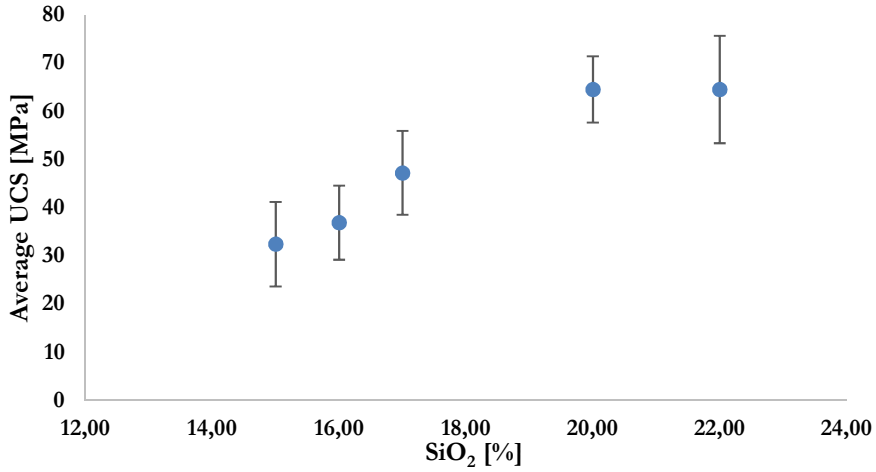

Fig. 9. Effect of silicate content on compressive strength.

Water Absorption and Porosity

The porosity as a function of total silica content in the binder was measured, and is shown in Figure 10. There is a sharp decrease in the porosity, when the silica content is increased by modification of sodium silicate modulus (Na4.3Si15-17). Similar result were reported by other researchers [50]. However, it was observed an increase in porosity when DE is increased (Na4.3Si20 and Na4.3Si22). This is most likely due to the availability of unreacted DE in the paste. DE is known to be a porous material [49, 51, 52], this characteristic could partly be liable for the increase porosity in the samples.

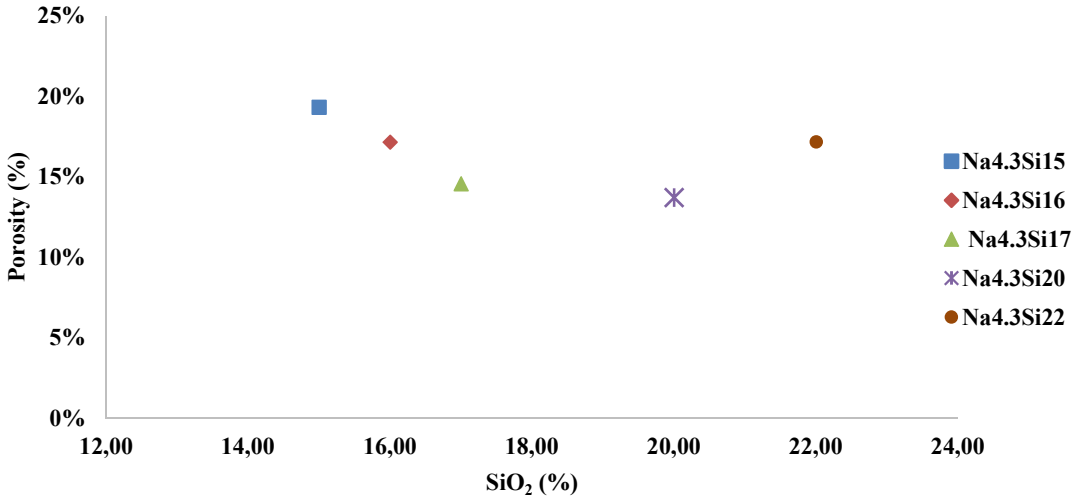

Fig. 10. Porosity as a function of the SiO_2 content

Water absorption analysis is an important parameter in applications of binders in construction. The water absorption and porosity of the AALS samples were measured, and the relationship between the two factors is presented in Fig. 11. As can be seen in the figure, there was a direct relationship between the porosity and water absorption with a relatively high correlation coefficient ($R^2 = 0.7889$). As the porosity gradually increases, so does the water absorption of the analyzed samples. This increase results from the availability of pores for water intake into the interior cavity from the surface of the samples. Two outlier data points are from samples with added DE (DE_AALS), and their increased water absorption is attributed to the properties of the DE: it has been reported to swell when used in OPC concrete as a pozzolan [48], and is also a porous material where open vs. closed porosity may play a role.

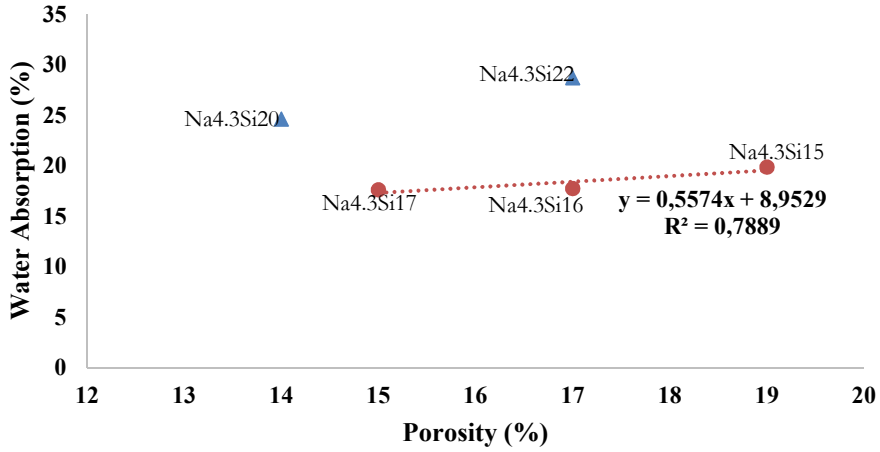

Fig. 11. Porosity–water absorption relationship of AALS specimens.

Conclusions

This study has investigated the use of milled LS from a Finnish steel factory as a precursor in alkali activation, considering the effects of alkali and silica contents on mechanical properties, water absorption and porosity of the produced samples. For the studied materials, an average UCS of up to 65 MPa after 28 days can be obtained through optimization of the silica and alkali metal contents. High alkali metal content reduces the compressive strength and the addition of DE as silica supplement enhances the strength of the paste. XRD analysis shows amorphous phases with major soluble crystalline phases identified as mayenite and dicalcium silicate (γ-C_2S) in the studied samples.

The reaction product was not identified using XRD, but using DRIFT spectra analysis, the spectra correspond to polymerized C-(N)-A-S-H gel and also suggest the occurrence of carbonation. Polished SEM shows dense microstructure with microcracks which developed during curing. Narrow reaction rings around unreacted slag grains indicates reactivity of the ladle slag in the alkaline activator solution.

The utilization of this highly crystalline slag as a sole precursor in alkali activation is promising, however it is essential to further analyze the durability of the alkali-activated ladle slag as well as the effect of aggregates on the properties of the AALS specimen; these subject areas are the focus of a forthcoming study.

Acknowledgements

This work was supported by the European Regional Development Fund (project code: A70189) and the following Finnish companies: Ekokem Oy, SSAB Europe Oy, Stora Enso Oyj, Pohjolan Voima Oy and Oulun Energia. Jarno Karvonen and Jani Österlund are acknowledged for their contributions to the laboratory analyses.

References

1. 2012: Euroslag. http://www.euroslag.com/products/statistics/2012/. Accessed 8 Mar 2016

2. Serjun VZ, Mirtič B, Mladenovič A (2013) Evaluation of ladle slag as a potential material for building and civil engineering. Mater Tehnol 47:543–550.

3. Tracz T, Hager I, Sideris KK, et al (2015) 7th Scientific-Technical Conference on Material Problems in Civil Engineering MATBUD'2015Production of Durable Self-compacting Concrete Using Ladle Furnace Slag (LFS) as Filler Material. Procedia Eng 108:592–597. doi: 10.1016/j.proeng.2015.06.184

4. Manso JM, Rodriguez Á, Aragón Á, Gonzalez JJ (2011) The durability of masonry mortars made with ladle furnace slag. Constr Build Mater 25:3508–3519. doi: 10.1016/j.conbuildmat.2011.03.044

5. Manso JM, Losañez M, Polanco JA, Gonzalez JJ (2005) Ladle Furnace Slag in Construction. J Mater Civ Eng 17:513–518. doi: 10.1061/(ASCE)0899-1561(2005)17:5(513)

6. Andreas L, Diener S, Lagerkvist A (2014) Steel slags in a landfill top cover – Experiences from a full-scale experiment. Waste Manag 34:692–701. doi: 10.1016/j.wasman.2013.12.003

7. Koizumi S, Miki T, Nagasaka T (2015) Enrichment of Phosphorus Oxide in Steelmaking Slag by Utilizing Capillary Action. J Sustain Metall 1–6. doi: 10.1007/s40831-015-0035-3

8. Buchwald A, Hilbig H, Kaps C (2007) Alkali-activated metakaolin-slag blends—performance and structure in dependence of their composition. J Mater Sci 42:3024–3032. doi: 10.1007/s10853-006-0525-6

9. Guerrieri M, Sanjayan J, Collins F (2009) Residual strength properties of sodium silicate alkali activated slag paste exposed to elevated temperatures. Mater Struct 43:765–773. doi: 10.1617/s11527-009-9546-3

10. Guerrieri M, Sanjayan JG (2010) Behavior of combined fly ash/slag-based geopolymers when exposed to high temperatures. Fire Mater 34:163–175. doi: 10.1002/fam.1014

11. Provis JL, Bernal SA (2014) Geopolymers and Related Alkali-Activated Materials. Annu Rev Mater Res 44:299–327. doi: 10.1146/annurev-matsci-070813-113515

12. Pacheco-Torgal F, Labrincha J, Leonelli C, et al (2014) Handbook of Alkali-Activated Cements, Mortars and Concretes. Elsevier

13. Yip CK, Lukey GC, Provis JL, van Deventer JSJ (2008) Effect of calcium silicate sources on geopolymerisation. Cem Concr Res 38:554–564. doi: 10.1016/j.cemconres.2007.11.001

14. Myers RJ, Bernal SA, San Nicolas R, Provis JL (2013) Generalized Structural Description of Calcium–Sodium Aluminosilicate Hydrate Gels: The Cross-Linked Substituted Tobermorite Model. Langmuir 29:5294–5306. doi: 10.1021/la4000473

15. Provis JL (2013) Geopolymers and other alkali activated materials: why, how, and what? Mater Struct 47:11–25. doi: 10.1617/s11527-013-0211-5

16. Chi M (2012) Effects of dosage of alkali-activated solution and curing conditions on the properties and durability of alkali-activated slag concrete. Constr Build Mater 35:240–245. doi: 10.1016/j.conbuildmat.2012.04.005

17. Bignozzi MC, Manzi S, Lancellotti I, et al (2013) Mix-design and characterization of alkali activated materials based on metakaolin and ladle slag. Appl Clay Sci 73:78–85. doi: 10.1016/j.clay.2012.09.015

18. Shi C (2002) Characteristics and cementitious properties of ladle slag fines from steel production. Cem Concr Res 32:459–462. doi: 10.1016/S0008-8846(01)00707-4

19. Salman M, Cizer Ö, Pontikes Y, et al (2015) Cementitious binders from activated stainless steel refining slag and the effect of alkali solutions. J Hazard Mater 286:211–219. doi: 10.1016/j.jhazmat.2014.12.046

20. Salman M, Cizer Ö, Pontikes Y, et al (2014) Effect of curing temperatures on the alkali activation of crystalline continuous casting stainless steel slag. Constr Build Mater 71:308–316. doi: 10.1016/j.conbuildmat.2014.08.067

21. Kriskova L, Pontikes Y, Cizer Ö, et al (2012) Effect of mechanical activation on the hydraulic properties of stainless steel slags. Cem Concr Res 42:778–788. doi: 10.1016/j.cemconres.2012.02.016

22. Kriskova L, Pontikes Y, Zhang F, et al (2014) Influence of mechanical and chemical activation on the hydraulic properties of gamma dicalcium silicate. Cem Concr Res 55:59–68. doi: 10.1016/j.cemconres.2013.10.004

23. Salman M, Cizer Ö, Pontikes Y, et al (October 1, 2015b) Alkali Activation of AOD Stainless Steel Slag Under Steam Curing Conditions. J Am Ceram Soc 98:3062–3074. doi: 10.1111/jace.13776

24. Lancellotti I, Ponzoni C, Bignozzi MC, et al (2014) Incinerator bottom ash and ladle slag for geopolymers preparation. Waste Biomass Valorization 5:393–401. doi: 10.1007/s12649-014-9299-2

25. Natali Murri A, Rickard WDA, Bignozzi MC, Van Riessen A (2013) High temperature behaviour of ambient cured alkali-activated materials based on ladle slag. Cem Concr Res 43:51–61. doi: 10.1016/j.cemconres.2012.09.011

26. Natali A, Manzi S, Bignozzi MC (2011) Novel fiber-reinforced composite materials based on sustainable geopolymer matrix. Procedia Eng 21:1124–1131. doi: 10.1016/j.proeng.2011.11.2120

27. Bignozzi MC, Manzi S, Lancellotti I, et al (2013) Mix-design and characterization of alkali activated materials based on metakaolin and ladle slag. Appl Clay Sci 73:78–85. doi: 10.1016/j.clay.2012.09.015

28. Bougara A, Lynsdale C, Ezziane K (2009) Activation of Algerian slag in mortars. Constr Build Mater 23:542–547. doi: 10.1016/j.conbuildmat.2007.10.012

29. Torgal FP, Jalali S (2011) Eco-efficient Construction and Building Materials. Springer Science & Business Media

30. SFS Online (2009) SFS 5513 - Brick Tile Testing (Finnish standard). https://online.sfs.fi/fi/index/tuotteet/SFS/SFS/ID2/5/119637.html.stx. Accessed 22 Dec 2015

31. Garcia-Lodeiro I, Palomo A, Fernández-Jiménez A (2014) An overview of the chemistry of alkali-activated cement-based binders. In: Handb. Alkali-Act. Cem. Mortars Concr. pp 19–47

32. Chang JJ (2003) A study on the setting characteristics of sodium silicate-activated slag pastes. Cem Concr Res 33:1005–1011. doi: 10.1016/S0008-8846(02)01096-7

33. Kuo W-T, Hou T-C (2014) Engineering properties of alkali-activated binders by use of desulfurization slag and GGBFS. Constr Build Mater 66:229–234. doi: 10.1016/j.conbuildmat.2014.05.056

34. Majumbar AJ, Singh B, Edmonds RN (1989) Hydration of mixtures of C12A7 and granulated blastfurnace slag. Cem Concr Res 19:848–856. doi: 10.1016/0008-8846(89)90097-5

35. Adolfsson D, Robinson R, Engström F, Björkman B (2011) Influence of mineralogy on the hydraulic properties of ladle slag. Cem Concr Res 41:865–871. doi: 10.1016/j.cemconres.2011.04.003

36. Collins F, Sanjayan JG (1999) Strength and shrinkage properties of alkali-activated slag concrete containing porous coarse aggregate. Cem Concr Res 29:607–610. doi: 10.1016/S0008-8846(98)00203-8

37. Shi C, Roy D, Krivenko P (2006) Alkali-Activated Cements and Concretes. CRC Press

38. Nikolić I, Drinčić A, Djurović D, et al (2016) Kinetics of electric arc furnace slag leaching in alkaline solutions. Constr Build Mater 108:1–9. doi: 10.1016/j.conbuildmat.2016.01.038

39. Yu P, Kirkpatrick RJ, Poe B, et al (1999) Structure of Calcium Silicate Hydrate (C-S-H): Near-, Mid-, and Far-Infrared Spectroscopy. J Am Ceram Soc 82:742–748. doi: 10.1111/j.1151-2916.1999.tb01826.x

40. Lecomte I, Henrist C, Liégeois M, et al (2006) (Micro)-structural comparison between geopolymers, alkali-activated slag cement and Portland cement. J Eur Ceram Soc 26:3789–3797. doi: 10.1016/j.jeurceramsoc.2005.12.021

41. Zhang Z, Wang H, Provis JL, et al (2012) Quantitative kinetic and structural analysis of geopolymers. Part 1. The activation of metakaolin with sodium hydroxide. Thermochim Acta 539:23–33.

42. Gao X, Yu QL, Brouwers HJH (2015) Characterization of alkali activated slag–fly ash blends containing nano-silica. Constr Build Mater 98:397–406. doi: 10.1016/j.conbuildmat.2015.08.086

43. Garcia-Lodeiro I, Palomo A, Fernández-Jiménez A, Macphee DE (2011) Compatibility studies between N-A-S-H and C-A-S-H gels. Study in the ternary diagram Na2O–CaO–Al2O3–SiO2–H2O. Cem Concr Res 41:923–931. doi: 10.1016/j.cemconres.2011.05.006

44. Bernal SA, Provis JL, Rose V, Mejía de Gutierrez R (2011) Evolution of binder structure in sodium silicate-activated slag-metakaolin blends. Cem Concr Compos 33:46–54. doi: 10.1016/j.cemconcomp.2010.09.004

45. Kupaei RH, Alengaram UJ, Jumaat MZ, et al (2014) The Effect of Different Parameters on the Development of Compressive Strength of Oil Palm Shell Geopolymer Concrete, The Effect of Different Parameters on the Development of Compressive Strength of Oil Palm Shell Geopolymer Concrete. Sci World J Sci World J 2014, 2014:e898536. doi: 10.1155/2014/898536, 10.1155/2014/898536

46. Qureshi N, Ghosh S, Mohd (2013) Effect of Alkali Content on Strength and Microstructure of GGBFS Paste. Glob. J. Res. Eng. 13:

47. Zhang Z, Yang T, Wang H (2014) The effect of efflorescence on the mechanical properties of fly ash-based geopolymer binders. 23rd Australas Conf Mech Struct Mater ACMSM23 107–112.

48. Posi P, Lertnimoolchai S, Sata V, Chindaprasirt P (2013) Pressed lightweight concrete containing calcined diatomite aggregate. Constr Build Mater 47:896–901. doi: 10.1016/j.conbuildmat.2013.05.094

49. Jud Sierra E, Miller SA, Sakulich AR, et al (2010) Pozzolanic Activity of Diatomaceous Earth. J Am Ceram Soc 93:3406–3410. doi: 10.1111/j.1551-2916.2010.03886.x

50. Qureshi MN, Ghosh S (2014) Effect of Silicate Content on the Properties of Alkali-Activated Blast Furnace Slag Paste. Arab J Sci Eng 39:5905–5916. doi: 10.1007/s13369-014-1172-x

51. Petrović DV, Mitrović ČB, Trišovic NR, Golubović ZZ (2011) On the Particles Size Distributions of Diatomaceous Earth and Perlite Granulations. Stroj Vestn – J Mech Eng 57:843–850. doi: 10.5545/sv-jme.2010.050

52. Pimraksa K, Chindaprasirt P (2009) Lightweight bricks made of diatomaceous earth, lime and gypsum. Ceram Int 35:471–478. doi: 10.1016/j.ceramint.2008.01.013